

Revealing laser-coherent electron features using phase-of-the-phase spectroscopy

V.A. Tulsy¹, B. Krebs¹, J. Tiggesbäumker^{1,2}, D. Bauer¹

¹ Institute of Physics, University of Rostock, 18051 Rostock, Germany

² Department Life, Light and Matter, University of Rostock, 18051 Rostock, Germany

Abstract. Phase-of-the-phase (PoP) spectroscopy is extended to two-color laser fields having a circularly counter-rotating polarization. In particular, the higher harmonics of the (two-color) phase information are analyzed in order to extract the laser-coherent part of the photoelectron spectra taken under complex target conditions. We illustrate this with a proof-of-principle simulation by considering strong-field electron emission from argon atoms within helium nanodroplets under realistic experimental conditions, i.e., a limited number of photoemission events. Multiple elastic scattering on neutral helium atoms creates a laser-incoherent background, but the higher harmonics of the PoP-signal allow to resolve the coherent contribution to the photoemission.

1. Introduction

Photoelectron momentum distributions obtained in experiments with strong laser fields are a treasury containing valuable information related to the target, the laser field, and the ultrafast phenomena during the process of ionization. However, in complex targets scattering may destroy the phase relation between the photoelectron yield and the laser field, and these electrons may clutter the coherent electron spectral features known from atomic gas-phase targets (such as plateaus, low-energy structures etc.). The recently proposed phase-of-the-phase (PoP) technique [1] can serve as Occam’s razor with respect to incoherent processes that spoil photoelectron spectra (PES). The general principle of the PoP and similar techniques is based on the irradiation of a target with a laser field that has a periodic parameter such as the relative phase between two fields with different colors [1–9] or the carrier-envelope phase [10]. However, in contrast to techniques where the forward-backward asymmetry [11–16] or side streaking [17–22] of the PES is analyzed at selected values of the periodic parameter, the PoP suggests to perform the Fourier transform with respect to this periodic parameter and to reveal how the PES follow it, e.g., whether the PES change with the same periodicity as the relative phase (“first harmonic”) but a certain phase lag Φ_1 (the “phase of the phase”), twice per period (“second harmonic”, with the corresponding phase lag Φ_2), and so on. It turns out that these Fourier components have well distinguished features at certain momenta. Specifically, the phase lag of some momentum-resolved Fourier components sharply flips along certain curves in momentum-space. Those “flipping curves” are sensitive to the parameters of the system, i.e., the laser intensity and frequency, and the type of target used.

In Ref. [9], the PoP technique was developed for the case of two-color circularly polarized counter-rotating intense laser fields with frequency ratio 1:2. Here, we extend the method to arbitrary ratios. We establish the general property of the PoP flipping curves, showing that they all have a quite simple, circular geometry and therefore are easier to analyze than, for instance, the features observed in the PES for two-color linearly polarized fields [1, 2]. One of the flipping curves was predicted in [9]. However, for fast photoelectrons, where the signals are low as a consequence of the significantly reduced ionization

probability, flipping curves may not be resolved due to the small number of events on the detector. In the present paper, we propose a way to bypass this problem extending the theory so that it can be used for a broader domain of parameters. We choose the specific frequency ratio ω - 2ω in our examples, as it is widely used in both experimental and theoretical investigations [23–29]. Note, however, that for other frequency ratios $a\omega$ - $b\omega$, being of particular interest nowadays (see, e.g., [30–34]), the PoP technique can also be applied.

The paper is organized as follows. Section 2 is devoted to the derivation of the relevant formulas within the Strong Field Approximation (SFA) [35–37], and the general properties of PoP spectra are derived. In Section 3, the PES obtained for a complex target where multiple elastic scattering of electrons after ionization are taken into account is presented. Elastic scattering gives rise to a huge contribution of the incoherent electron signal (with respect to the phase shift between the laser field components). The PoP technique is then applied in order to reveal the small coherent features in the electron yield. We conclude in Section 4. Atomic units are used throughout this paper unless otherwise stated.

2. Theory

2.1. Strong field approximation

Let the vector potential of a laser field in dipole approximation be of the form

$$\mathbf{A}(t) = \mathbf{A}_a(a\omega t) + \mathbf{A}_b(b\omega t + \phi). \quad (1)$$

The PoP technique is based on the momentum-resolved PES, Fourier-transformed with respect to the phase shift ϕ between the laser field components,

$$Y(\mathbf{p}, \phi) = Y_0(\mathbf{p}) + |Y_1(\mathbf{p})|e^{i\phi + i\Phi_1(\mathbf{p})} + |Y_2(\mathbf{p})|e^{i2\phi + i\Phi_2(\mathbf{p})} + \dots + \text{c.c.} \quad (2)$$

The phases $\Phi_n(\mathbf{p}) = \arg Y_n(\mathbf{p})$ describe the phase lag of the change in the photoelectron yield as a function of the relative phase ϕ , hence the name “phase(s) of the phase”. In the previous papers Ref. [1, 2, 9], only $\Phi_1(\mathbf{p})$ was considered. A visual representation of the series (2) is shown in Fig. 1. The curves $Y_n(\mathbf{p}) = 0$ in momentum space are very sensitive to the parameters of the system under consideration. Let us derive simple, analytical properties of $Y_n(\mathbf{p})$ using the strong

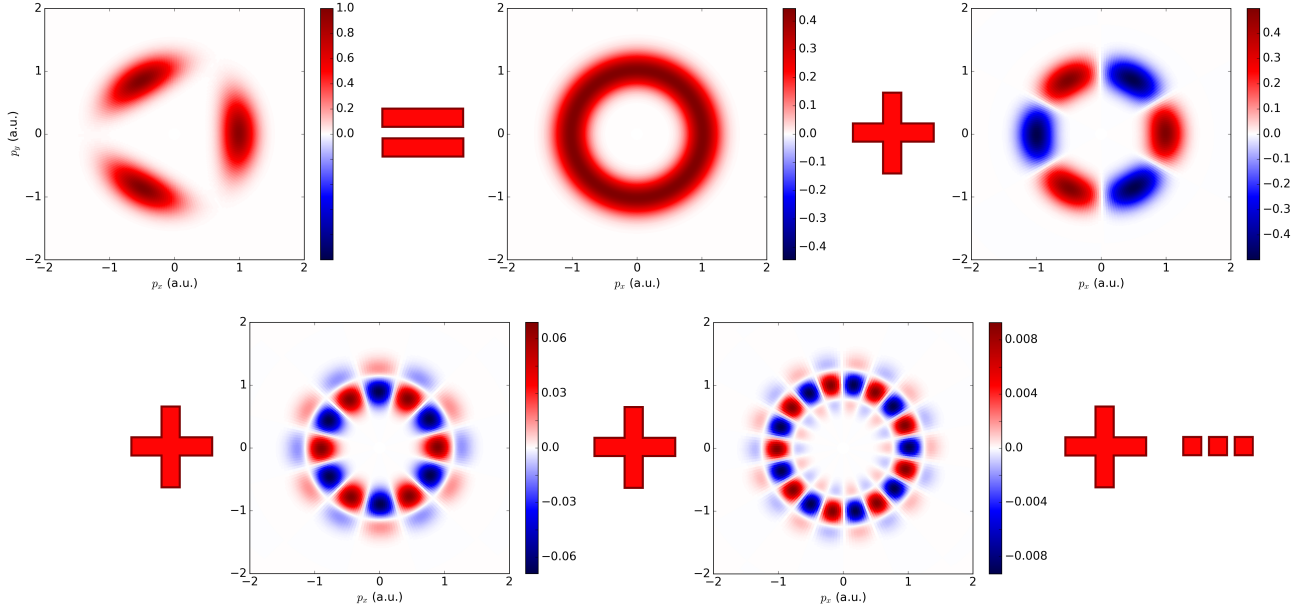


Figure 1. Decomposition of a total photoelectron spectrum into Fourier components with respect to the phase shift between the two colors of the laser field (calculated according to (5) with interference terms discarded). The laser field defined by (7) with $a = 1, b = 2$, intensity and wavelength of the main component of the laser $I = 2 \cdot 10^{14} \text{ W/cm}^2$, $\lambda_1 = 800 \text{ nm}$, $\xi = 0.05$, $\phi = 0$, and ionization potential $I_p = 15.8 \text{ eV}$ (argon).

field approximation (SFA) [35–37]. Within the SFA, we can write the photoionization rate as

$$Y = \left| \int_0^T P(\mathbf{p}, t) e^{iS(t)} dt \right|^2 \quad (3)$$

where T is a laser period. The function $S(t)$ in the exponent

$$S(t) = \int_0^t \left[\frac{(\mathbf{p} + \mathbf{A}(t'))^2}{2} + I_p \right] dt' \quad (4)$$

is the classical action of the photoelectron with final momentum \mathbf{p} , $\mathbf{A}(t)$ is the vector potential determining the laser electric field $\mathbf{E}(t) = -\partial_t \mathbf{A}(t)$, and I_p is the ionization potential.

We calculate the yield (3) with exponential accuracy using the saddle-point method (see, e.g. [38–40] and references therein) and obtain

$$Y(\mathbf{p}, \phi) \sim \left| \sum_s e^{iS(t_s)} \right|^2 \quad (5)$$

where the complex times t_s are solutions to the saddle-point equation

$$\frac{(\mathbf{p} + \mathbf{A}(t_s))^2}{2} + I_p = 0. \quad (6)$$

In the present paper, we aim at the case of two-color, circularly polarized, counter-rotating fields described by a vector potential of the form

$$\begin{aligned} A_x(t) &= A_0 [\cos(awt) + \xi \cos(bwt + \phi)], \\ A_y(t) &= A_0 [\sin(awt) - \xi \sin(bwt + \phi)], \end{aligned} \quad (7)$$

and $A_z = 0$, with the second component being weak ($\xi \ll 1$), and a, b coprime, and $b > a$. For the sake of simplicity, we assume an infinitely long pulse with a constant envelope $A_0 = E_0/a\omega$, where E_0 is the amplitude of the main (i.e., strong) component of the laser field.

Introducing the Keldysh parameter $\gamma = \sqrt{2I_p}/A_0$ and a dimensionless momentum $\mathbf{q} = \mathbf{p}/A_0$, one can rewrite (6) as

$$0 = 1 + \gamma^2 + q^2 + \xi^2 + 2q \cos(awt_s - \alpha) + 2\xi[q \cos(bwt_s + \alpha + \phi) + \cos((a+b)\omega t_s + \phi)]. \quad (8)$$

Here, α is the angle of photoelectron emission in the xy plane, i.e.,

$$\mathbf{q} = q(\mathbf{e}_x \cos \alpha + \mathbf{e}_y \sin \alpha). \quad (9)$$

Most electrons will be emitted within the xy plane as long as non-dipole effects are negligible [37, 41]. Hence we do not consider final photoelectron momenta out of the xy plane in this work.

In the monochromatic case ($\xi = 0$), the emission is isotropic with respect to the angle α [41] (see also [42]). Therefore, it is convenient to introduce a new variable

$$a\tau = awt - \alpha. \quad (10)$$

In the two-color case, it is useful to introduce additionally

$$a\theta = (a+b)\alpha + a\phi. \quad (11)$$

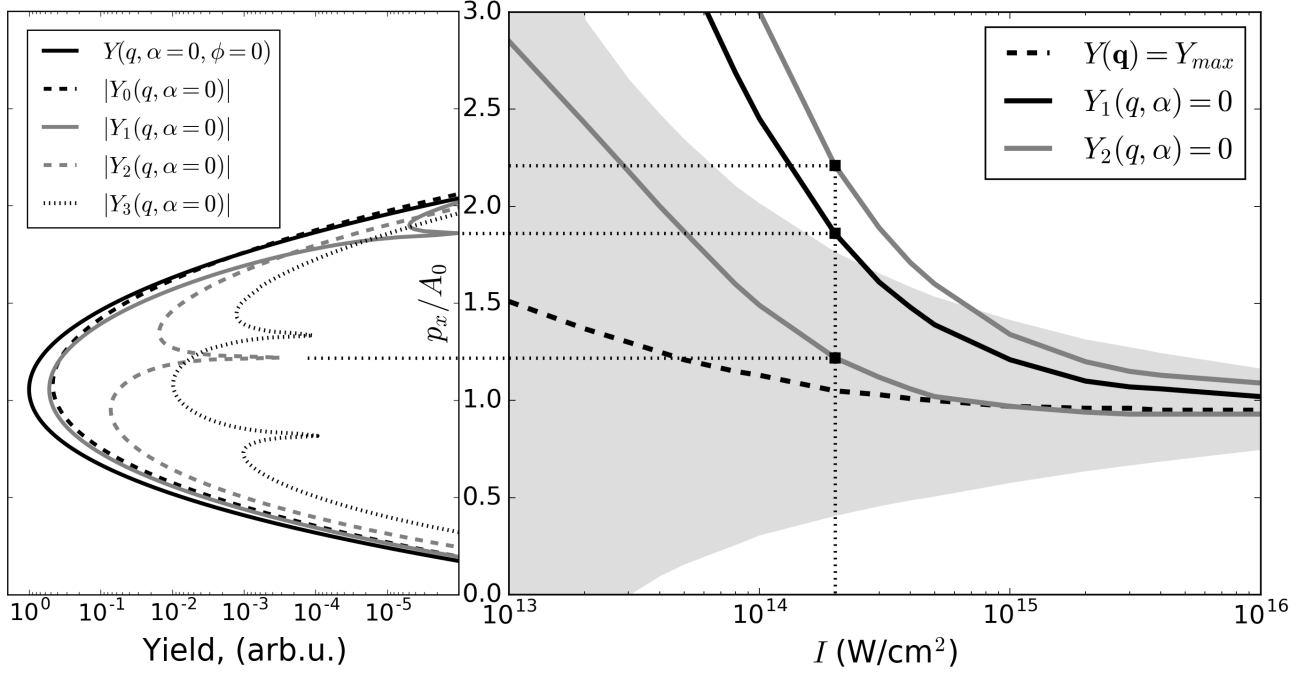


Figure 2. Left panel: Total yield Y and absolute values of several of the Fourier components Y_n for $n = 0-3$, taken along the $q_x = p_x/A_0 > 0$ direction. All parameters are the same as in Fig.1. Spiky minima correspond to momenta where the phase flipping occurs and are indicated by squares on the right panel. Right panel: Radial momenta of the Fourier expansion for argon in a two-color ω - 2ω laser field with the laser main component's wavelength $\lambda_1 = 800$ nm plotted versus the intensity of that laser field. The gray area represents a domain with a yield above 0.1% of its maximum, and the dashed line indicates the position of this maximum.

One can then rewrite (8) as

$$0 = 1 + \gamma^2 + q^2 + \xi^2 + 2q \cos(a\tau_s) + 2\xi[q \cos(b\tau_s + \theta) + \cos((a+b)\tau_s + \theta)], \quad (12)$$

and the action (4) as

$$S(\tau_s) = \frac{A_0^2}{2a\omega} \left[(1 + \gamma^2 + q^2 + \xi^2)a\tau + 2q \sin(a\tau) + 2\xi \left(q \frac{a}{b} \sin(b\tau + \theta) + \frac{a}{a+b} \sin((a+b)\tau + \theta) \right) \right] \Bigg|_{\tau=0}^{\tau=\tau_s}. \quad (13)$$

The yield only depends on α and ϕ in the combination (11). The coefficient in front of α in (11) is related to the $(a+b)$ -fold symmetry of the electric field and, hence, of the vector potential and the yield. As a consequence, the yield has the property

$$Y(q, \alpha, \phi) = Y\left(q, \alpha + \frac{a}{a+b}\phi, 0\right) = Y\left(q, 0, \phi + \frac{a+b}{a}\alpha\right). \quad (14)$$

2.2. General properties of the phase-of-the-phase

Now let us pass over to the main quantity of interest, namely, the Fourier components of the yield

$$Y_n(q, \alpha) = \int_0^{2\pi} Y(q, \alpha, \phi) e^{-in\phi} d\phi. \quad (15)$$

Property (14) suggests to factor out the α -dependence of each Y_n ,

$$Y_n(q, \alpha) = Y_n(q, 0) e^{in \frac{a+b}{a} \alpha}. \quad (16)$$

Another general property of the Y_n is revealed if we consider the action and the saddle-point equation. One may easily verify that if $t_s(p, \alpha = 0, \phi)$ is a solution to (12) for a given ϕ , then $t_s(\alpha = 0, -\phi) = 2\pi a - t_s^*(p, \alpha = 0, \phi)$ is a solution for $-\phi$. Next, inserting these solutions into the action (13) and evaluating the imaginary part of it, one obtains the same value in both cases, i.e., $\Im S(\phi, t_s(\alpha = 0, \phi)) = \Im S(-\phi, t_s(\alpha = 0, -\phi))$. Thus, the yield is symmetric in ϕ for $\alpha = 0$. This allows to rewrite (15) as

$$Y_n(q, \alpha) = 2 \int_0^\pi Y(q, 0, \phi) \cos(n\phi) d\phi e^{in \frac{a+b}{a} \alpha}. \quad (17)$$

Finally, let us pass to the arguments $\Phi_n = \arg Y_n$ of these Fourier components (i.e., to phases-of-the-phase) that can now be written as

$$\Phi_n(q, \alpha) = n \frac{a+b}{a} \alpha + \pi \delta_n(q). \quad (18)$$

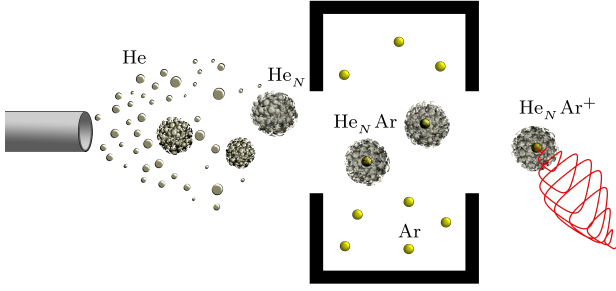


Figure 3. Sketch of the setup used in our calculations. Each helium droplet of size N captures a single argon atom, which is then ionized by a ω - 2ω laser field.

Here, $\delta_n(q)$ is related to the sign of the purely real $Y_n(q, 0)$ and can only have values equal to 0 for $Y_n(q, 0) > 0$ or 1 for $Y_n(q, 0) < 0$ (without loss of generality). Expression (18) highlights an essential advantage of the PoP technique related to circular, counter-rotating fields: the only type of momentum-dependent features that appear in the PoP spectra are circles centered around $q = 0$ at which the phase has a sharp flip of π . This makes the PoP flipping curves one dimension simpler compared to the case of linear+linear two-color fields and allows to represent their behavior for a broad variety of parameters within a single plot (see the example shown in Fig.2), thus making PoP a possibly handy laser-calibration technique.

2.3. PoP flipping of the higher Fourier components

Electron emission in circularly polarized fields at intensities above 10^{14} W/cm² and $I_p/\omega \gg 1$ has the highest probability for radial momentum $q = 1$, i.e., $p = A_0 = E_0/a\omega$ [41]. In Ref. [9], the position of the flipping of the PoP of the first Fourier component Φ_1 for ω - 2ω laser fields (i.e., $a = 1, b = 2$ in the current notation) has been analytically described. It appeared that the circle of the Φ_1 flipping is in general located in the momentum space region far beyond the peak of the ionization probability where the yield might be too low in actual measurements. Here we show that in such cases the PoP technique using higher harmonics of the Fourier expansion should be more practicable from the experimental point of view. In particular, for the laser parameters considered above, Φ_2 flips close to the maximum yield (see example in Fig.2) and, thus, should be easier to observe than the flipping of Φ_1 .

3. PoP-based exclusion of incoherent scattering

In order to demonstrate another practical application of the PoP technique, we introduce a model

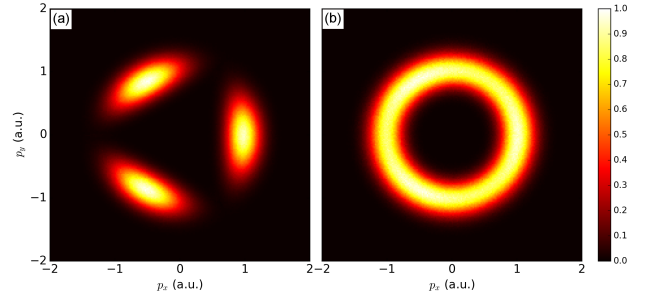


Figure 4. Comparison of PES obtained within the SFA for bare (a) and embedded (b) argon in the circularly polarized, counter-rotating ω - 2ω field. In (b), helium droplets of size $N = 3 \cdot 10^3$ are considered, which leads to a blurring of the PES due to elastic e-He scattering. Intensity and wavelength of the main component of the laser $I = 2 \cdot 10^{14}$ W/cm² and $\lambda_1 = 800$ nm, $\xi = 0.05$, $\phi = 0$. $N_e = 2 \cdot 10^7$ photoelectrons are simulated.

describing the PES generated by ionization of atoms in a complex environment. In particular, we consider helium nanodroplets [43]. They are widely used as finite spectroscopic matrices for embedded particles, called dopants [44–48]. The ultralow temperature of the droplets, the weak electronic interaction between dopant and helium, and the optical transparency up to about 20 eV allows for almost undisturbed high resolution spectroscopy in the microwave, IR and UV spectral range of targets varying in complexity from simple atoms [49] to large biomolecules [49–51]. In contrast, photoelectrons emitted by the dopant might scatter on the surrounding helium atoms before leaving the droplet. In that way, an incoherent electron yield is added to the PES since the phase information is almost lost in the scattering. This incoherent contribution might mask the interesting, laser-coherent features in the ordinary PES while PoP spectra still show them, as will be demonstrated in the following.

In our computer experiment, we use argon as the dopant. The laser parameters considered are as follows: two counter-rotating, circularly polarized components with wavelengths 800 nm and 400 nm ($a = 1, b = 2$), intensities are $I_1 = 2 \cdot 10^{14}$ W/cm² and $I_2 = 2 \cdot 10^{12}$ W/cm² ($\xi = 0.05$). A sketch of the experimental setup to produce single-atom-doped helium droplets is shown in Fig.3. We consider droplets of size $D \approx 60$ Å, that is $N \approx 3 \cdot 10^3$ atoms. At 20 bar and for a $5 \mu\text{m}$ diameter gas exit, nozzle temperatures of about 16 K have to be established [52]. The partial pressure of argon gas in the pick-up region is adjusted to conditions such that only a single Ar atom is present in each droplet on average.

The photoelectrons have a significant probability of multiple scattering on the enclosing neutral helium atoms before leaving the droplet and flying towards the detector. As the mean distance between the He is larger than their size, we treat each scattering within a

single-atom approach. Due to the significant difference between the ionization potentials of argon (15.8 eV) and helium (24.6 eV), we neglect the ionization probability of the latter and consider photoelectrons produced from argon only. For the sake of simplicity, we reduce our problem to the two-dimensional case, taking into account the polarization plane only, since most of the photoelectrons produced from an atom in a circularly polarized laser field have their momenta within the polarization plane. As a result, most of the coherent signal is in the momentum distribution in this plane. As typical kinetic energies of photoelectrons produced from argon with the chosen laser intensity are too low to ionize or excite helium, we only take elastic scattering into account. Moreover, most electrons have an energy close to the average $\langle p^2 \rangle / 2 = 15.4$ eV so that we neglect the dependence of the cross section on the energy of the scattered electrons. The total cross section σ and the angular distribution $d\sigma/d\Omega$ at $p^2/2 = 15$ eV are taken from [53]. For $N_\phi = 20$ phases $\phi \in [0, 2\pi[$ we simulate a finite number N_e of ionization events with the initial momentum distribution taken from the SFA. Then we simulate their scattering with the probability of traveling a distance s before a new scattering event as

$$w(s) = 1 - e^{-n\sigma s} \quad (19)$$

where the concentration of helium atoms n is assumed to be constant all over the droplet. Thus, s is chosen randomly as $s = -(n\sigma)^{-1} \log R$ where R is a random number between 0 to 1. If s is smaller than the distance to the boundary of the droplet, the scattering occurs. The angle of scattering ϑ is then chosen randomly in a range from $-\pi$ to π according to the angular distribution $d\sigma/d\Omega$. The total number of scattering events for each initial electron is not restricted.

An example of a PES obtained with the SFA is shown in Fig.4(a). If an atom is trapped inside a helium droplet the PES is significantly distorted because of electron-He scattering (see Fig.4(b)). The 3-fold symmetric laser-coherent part of the total signal is now deeply suppressed by an almost circular PES of multiply scattered electrons. The percentage of electrons as a function of the number of scattering events in Fig.5 shows that only about 6% of the laser-coherent signal survives. After having simulated a set of PES for different relative phases ϕ , we apply the PoP technique and obtain the phase flipping curves (see Fig.6). Due to the low ionization probability of photoelectrons with high momenta, the flipping curve for Φ_1 (which is at $p = 1.76$ a.u.) is only visible if a huge number of ionization events is considered ($N_e \geq 2 \cdot 10^8$ for a grid with $dp = 0.02$ a.u.) even without scattering taken into account. However, as previously noted, instead of increasing the number of particles (i.e., the measurement time in the experiment) one may

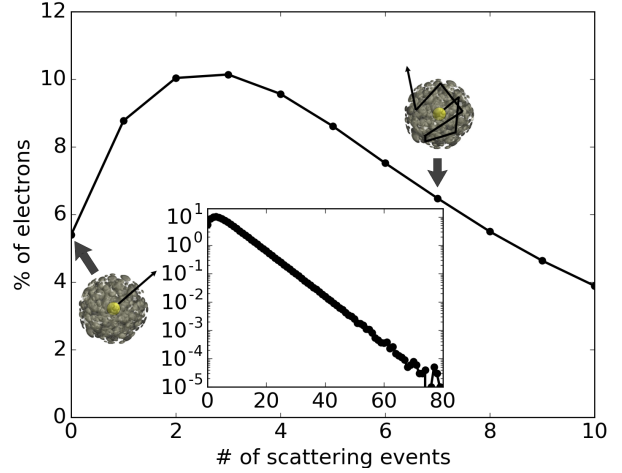


Figure 5. Percentage of the total number of photoelectrons $N_e = 2 \cdot 10^7$ that experienced a certain number of elastic scattering events before leaving the helium droplet. The inset shows the distribution logarithmically and over a wider range of scattering events.

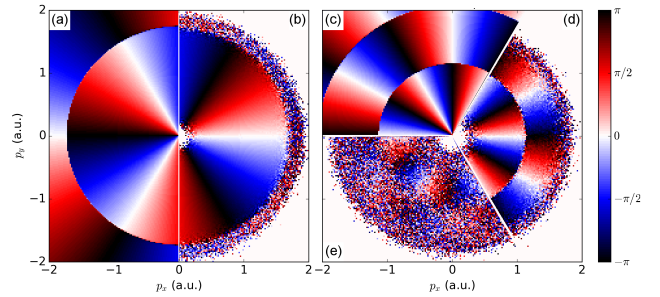


Figure 6. Phase-of-the-phase (a) Φ_1 predicted by the SFA. (b) Φ_1 obtained with a finite number of $N_e = 2 \cdot 10^8$ photoelectrons for each phase ϕ . (c) Φ_2 predicted by the SFA. (d) Φ_2 obtained with a finite number of $N_e = 2 \cdot 10^7$ photoelectrons for each phase ϕ . (e) Same as (d) but with elastic scattering on neutral helium atoms in the droplet taken into account. In each case $N_\phi = 20$ phases $\phi \in [0, 2\pi[$ have been simulated.

simply consider Φ_2 , the phase of the second harmonic in the Fourier expansion. As was predicted in Fig.2, it requires a significantly smaller N_e for the phase-flipping to remain visible, even when the spectra are distorted by scattering, as shown in Fig.6(e).

4. Conclusions

To wind up, we showed that a slight extension of the phase-of-the-phase technique applied to a two-color, circularly polarized and counter-rotating intense laser field can significantly improve its practicability: considering higher terms in the Fourier series of the photoelectron yield, phase-of-the-phase spectra with flipping curves that are located in regions of high photoelectron yield can be obtained. Being based on the observation of sharp and intensity-sensitive

features, phase-of-the-phase spectroscopy could be an instrument for accurately tuning and benchmarking the laser intensity.

Secondly, we performed a simulation of photoelectrons originating from the ionization of a single argon atom inside a helium droplet by a ω - 2ω laser field. The electrons may scatter on their way to the detector so that laser-coherent features in the photoelectron spectra are obscured. Simulating the spectra with a finite number of electrons mimics the effect of a finite measurement time and allowed to treat the effect of (multiple) scattering events on the electrons' pathways to the detector classically and statistically. Finally, we showed that laser-coherent features survive in the second-harmonic phase-of-the-phase spectrum calculated in such a manner.

Acknowledgments

This work was supported by the projects BA 2190/10, TI 210/7, and TI 210/8 of the German Science Foundation (DFG).

References

- [1] S. Skruszewicz, J. Tiggesbäumker, K.-H. Meiwes-Broer, M. Arbeiter, Th. Fennel, and D. Bauer. Two-color strong-field photoelectron spectroscopy and the phase of the phase. *Phys. Rev. Lett.*, 115:043001, Jul 2015.
- [2] M A Almajid, M Zabel, S Skruszewicz, J Tiggesbäumker, and D Bauer. Two-color phase-of-the-phase spectroscopy in the multiphoton regime. *Journal of Physics B: Atomic, Molecular and Optical Physics*, 50(19):194001, 2017.
- [3] D Würzler, N Eicke, M Möller, D Seipt, A M Sayler, S Fritzsche, M Lein, and G G Paulus. Velocity map imaging of scattering dynamics in orthogonal two-color fields. *Journal of Physics B: Atomic, Molecular and Optical Physics*, 51(1):015001, nov 2017.
- [4] S. Beaulieu, A. Comby, A. Clergerie, J. Caillat, D. Descamps, N. Dudovich, B. Fabre, R. Généaux, F. Légaré, S. Petit, B. Pons, G. Porat, T. Ruchon, R. Taïeb, V. Blanchet, and Y. Mairesse. Attosecond-resolved photoionization of chiral molecules. *Science*, 358(6368):1288–1294, 2017.
- [5] Jia Tan, Yang Li, Yueming Zhou, Mingrui He, Yinbo Chen, Min Li, and Peixiang Lu. Identifying the contributions of multiple-returning recollision orbits in strong-field above-threshold ionization. *Optical and Quantum Electronics*, 50(2):57, Jan 2018.
- [6] Meng Han, Peipei Ge, Yun Shao, Qihuang Gong, and Yunquan Liu. Attoclock photoelectron interferometry with two-color corotating circular fields to probe the phase and the amplitude of emitting wave packets. *Phys. Rev. Lett.*, 120:073202, Feb 2018.
- [7] G. Porat, G. Alon, S. Rozen, O. Pedatzur, M. Krüger, D. Azoury, A. Natan, G. Orenstein, B. D. Bruner, M. J. J. Vrakking, and N. Dudovich. Attosecond time-resolved photoelectron holography. *Nature Communications*, 9(1), July 2018.
- [8] Jia Tan, Yueming Zhou, Min Li, Mingrui He, Yali Liu, and Peixiang Lu. Accurate measurement of laser intensity using photoelectron interference in strong-field tunneling ionization. *Opt. Express*, 26(16):20063–20075, Aug 2018.
- [9] V. A. Tulsy, M. A. Almajid, and D. Bauer. Two-color phase-of-the-phase spectroscopy with circularly polarized laser pulses. *Phys. Rev. A*, 98:053433, Nov 2018.
- [10] Philipp Rupp, Lennart Seiffert, Qingcao Liu, Frederik Süßmann, Byungnam Ahn, Benjamin Förg, Christian G. Schäfer, Markus Gallei, Valerie Mondes, Alexander Kessel, Sergei Trushin, Christina Graf, Eckart Rühl, Jinwoo Lee, Min Su Kim, Dong Eon Kim, Thomas Fennel, Matthias F. Kling, and Sergey Zherebtsov. Quenching of material dependence in few-cycle driven electron acceleration from nanoparticles under many-particle charge interaction. *Journal of Modern Optics*, 64(10-11):995–1003, 2017.
- [11] Lennart Seiffert, Jörg Köhn, Christian Peltz, Matthias F. Kling, and Thomas Fennel. Signatures and mechanisms of plasmon-enhanced electron emission from clusters in few-cycle laser fields. *Journal of Physics B: Atomic, Molecular and Optical Physics*, 50(22):224001, 2017.
- [12] C.-Z. Gao, P. M. Dinh, P.-G. Reinhard, E. Suraud, and C. Meier. Forward-backward asymmetry of photoemission in c_{60} excited by few-cycle laser pulses. *Phys. Rev. A*, 95:033427, Mar 2017.
- [13] Siqiang Luo, Min Li, Hui Xie, Peng Zhang, Shengliang Xu, Yang Li, Yueming Zhou, Pengfei Lan, and Peixiang Lu. Angular-dependent asymmetries of above-threshold ionization in a two-color laser field. *Phys. Rev. A*, 96:023417, Aug 2017.
- [14] M. Kübel, C. Burger, R. Siemering, Nora G. Kling, B. Bergues, A. S. Alnaser, I. Ben-Itzhak, R. Moshhammer, R. de Vivie-Riedle, and M. F. Kling. Phase- and intensity-dependence of ultrafast dynamics in hydrocarbon molecules in few-cycle laser fields. *Molecular Physics*, 115(15-16):1835–1845, 2017.
- [15] Doron Azoury, Michael Krüger, Gal Orenstein, Henrik R. Larsson, Sebastian Bauch, Barry D. Bruner, and Nirit Dudovich. Self-probing spectroscopy of XUV photoionization dynamics in atoms subjected to a strong-field environment. *Nature Communications*, 8(1), Nov 2017.
- [16] Yinyu Zhang, Philipp Kellner, Daniel Adolph, Danilo Zille, Philipp Wustelt, Daniel Würzler, Slawomir Skruszewicz, Max Möller, A. Max Sayler, and Gerhard G. Paulus. Single-shot, real-time carrier-envelope phase measurement and tagging based on stereographic above-threshold ionization at short-wave infrared wavelengths. *Opt. Lett.*, 42(24):5150–5153, Dec 2017.
- [17] Nicolas Eicke and Manfred Lein. Extracting trajectory information from two-color strong-field ionization. *Journal of Modern Optics*, 64(10-11):981–986, 2017.
- [18] Xiaochun Gong, Cheng Lin, Feng He, Qiyang Song, Kang Lin, Qinying Ji, Wenbin Zhang, Junyang Ma, Peifen Lu, Yunquan Liu, Heping Zeng, Weifeng Yang, and Jian Wu. Energy-resolved ultrashort delays of photoelectron emission clocked by orthogonal two-color laser fields. *Phys. Rev. Lett.*, 118:143203, Apr 2017.
- [19] Xinhua Xie, Tian Wang, ShaoGang Yu, XuanYang Lai, Stefan Roither, Daniil Kartashov, Andrius Baltuska, XiaoJun Liu, André Staudte, and Markus Kitzler. Disentangling intracycle interferences in photoelectron momentum distributions using orthogonal two-color laser fields. *Phys. Rev. Lett.*, 119:243201, Dec 2017.
- [20] Xiaoyang Yu, Min Li, Meng Han, and Yunquan Liu. Controlling backward-scattering photoelectron holography by attosecond streaking. *Phys. Rev. A*, 98:013415, Jul 2018.
- [21] Martin Richter, Maksim Kunitski, Markus Schöffler, Till Jahnke, Lothar P. H. Schmidt, Min Li, Yunquan Liu, and Reinhard Dörner. Streaking temporal double-slit

- interference by an orthogonal two-color laser field. *Phys. Rev. Lett.*, 114:143001, Apr 2015.
- [22] Martin Richter, Maksim Kunitski, Markus Schöffler, Till Jahnke, Lothar Ph. H. Schmidt, and Reinhard Dörner. Ionization in orthogonal two-color laser fields: Origin and phase dependences of trajectory-resolved coulomb effects. *Phys. Rev. A*, 94:033416, Sep 2016.
- [23] Christopher A. Mancuso, Daniel D. Hickstein, Patrik Grychtol, Ronny Knut, Ofer Kfir, Xiao-Min Tong, Franklin Dollar, Dmitriy Zusin, Maithreyi Gopalakrishnan, Christian Gentry, Emrah Turgut, Jennifer L. Ellis, Ming-Chang Chen, Avner Fleischer, Oren Cohen, Henry C. Kapteyn, and Margaret M. Murnane. Strong-field ionization with two-color circularly polarized laser fields. *Phys. Rev. A*, 91:031402, Mar 2015.
- [24] S. Eckart, M. Richter, M. Kunitski, A. Hartung, J. Rist, K. Henrichs, N. Schlott, H. Kang, T. Bauer, H. Sann, L. Ph. H. Schmidt, M. Schöffler, T. Jahnke, and R. Dörner. Nonsequential double ionization by counterrotating circularly polarized two-color laser fields. *Phys. Rev. Lett.*, 117:133202, Sep 2016.
- [25] Christopher A. Mancuso, Daniel D. Hickstein, Kevin M. Dorney, Jennifer L. Ellis, Elvedin Hasović, Ronny Knut, Patrik Grychtol, Christian Gentry, Maithreyi Gopalakrishnan, Dmitriy Zusin, Franklin J. Dollar, Xiao-Min Tong, Dejan B. Milošević, Wilhelm Becker, Henry C. Kapteyn, and Margaret M. Murnane. Controlling electron-ion rescattering in two-color circularly polarized femtosecond laser fields. *Phys. Rev. A*, 93:053406, May 2016.
- [26] Denitsa Baykusheva, Md Sabbir Ahsan, Nan Lin, and Hans Jakob Wörner. Bicircular high-harmonic spectroscopy reveals dynamical symmetries of atoms and molecules. *Phys. Rev. Lett.*, 116:123001, Mar 2016.
- [27] Christopher A. Mancuso, Kevin M. Dorney, Daniel D. Hickstein, Jan L. Chaloupka, Xiao-Min Tong, Jennifer L. Ellis, Henry C. Kapteyn, and Margaret M. Murnane. Observation of ionization enhancement in two-color circularly polarized laser fields. *Phys. Rev. A*, 96:023402, Aug 2017.
- [28] David Ayuso, Piero Decleva, Serguei Patchkovskii, and Olga Smirnova. Strong-field control and enhancement of chiral response in bi-elliptical high-order harmonic generation: an analytical model. *Journal of Physics B: Atomic, Molecular and Optical Physics*, 51(12):124002, May 2018.
- [29] Á. Jiménez-Galán, N. Zhavoronkov, D. Ayuso, F. Morales, S. Patchkovskii, M. Schloz, E. Pisanty, O. Smirnova, and M. Ivanov. Control of attosecond light polarization in two-color bicircular fields. *Phys. Rev. A*, 97:023409, Feb 2018.
- [30] F. Mauger, A D Bandrauk, and T Uzer. Circularly polarized molecular high harmonic generation using a bicircular laser. *Journal of Physics B: Atomic, Molecular and Optical Physics*, 49(10):10LT01, may 2016.
- [31] D. B. Milošević and W. Becker. Improved strong-field approximation and quantum-orbit theory: Application to ionization by a bicircular laser field. *Phys. Rev. A*, 93:063418, Jun 2016.
- [32] Dino Habibović, Aner Čerkić, Mustafa Busuladžić, Azra Gazibegović-Busuladžić, Senad Odžak, Elvedin Hasović, and Dejan B. Milošević. Molecules in a bicircular strong laser field. *Optical and Quantum Electronics*, 50(5):214, Apr 2018.
- [33] D. B. Milošević. Atomic and molecular processes in a strong bicircular laser field. *Atoms*, 6(4), 2018.
- [34] Georgios Petros Katsoulis, Rudraditya Sarkar, and Agapi Emmanouilidou. Enhancing frustrated double ionisation with no electronic correlation in triatomic molecules using counter-rotating two-color circular laser fields. <http://arxiv/1908.06262>, 2019.
- [35] L. V. Keldysh. Ionization in the field of a strong electromagnetic wave. *Zh. Eksp. Teor. Fiz.*, 20:1307, 1965.
- [36] F H M Faisal. Multiple absorption of laser photons by atoms. *Journal of Physics B: Atomic and Molecular Physics*, 6(4):L89, 1973.
- [37] H. R. Reiss. Effect of an intense electromagnetic field on a weakly bound system. *Phys. Rev. A*, 22:1786–1813, Nov 1980.
- [38] D. B. Milošević, D. Bauer, and W. Becker. Quantum-orbit theory of high-order atomic processes in intense laser fields. *J. Mod. Opt.*, 53(1-2):125–134, 2006.
- [39] S V Popruzhenko. Keldysh theory of strong field ionization: history, applications, difficulties and perspectives. *Journal of Physics B: Atomic, Molecular and Optical Physics*, 47(20):204001, 2014.
- [40] Kasra Amini, Jens Biegert, Francesca Calegari, Alexis Chacón, Marcelo F Ciappina, Alexandre Dauphin, Dmitry K Efimov, Carla Figueira de Morisson Faria, Krzysztof Giergiel, and Piotr Gniewek. Symphony on strong field approximation. *Rep. Prog. Phys.*, 82(11):116001, 2019.
- [41] V. S. Popov A. M. Perelomov and M. V. Terentev. Ionization of atoms in an alternating electric field: II. *Sov. Phys. JETP*, 23:924, 1966.
- [42] Ingo Barth and Olga Smirnova. Nonadiabatic tunneling in circularly polarized laser fields: Physical picture and calculations. *Phys. Rev. A*, 84:063415, Dec 2011.
- [43] Manuel Barranco, Rafael Guardiola, Susana Hernández, Ricardo Mayol, Jesús Navarro, and Martí Pi. Helium nanodroplets: An overview. *Journal of Low Temperature Physics*, 142(1-2):1–81, January 2006.
- [44] J.P. Toennies and A.F. Vilesov. Superfluid helium droplets: A uniquely cold nanomatrix for molecules and molecular complexes. *Angewandte Chemie International Edition*, 43 (20):2622, 2004.
- [45] Frank Stienkemeier and Kevin K Lehmann. Spectroscopy and dynamics in helium nanodroplets. *Journal of Physics B: Atomic, Molecular and Optical Physics*, 39(8):R127–R166, April 2006.
- [46] Josef Tiggesbäumker and Frank Stienkemeier. Formation and properties of metal clusters isolated in helium droplets. *Phys. Chem. Chem. Phys.*, 9:4748–4770, 2007.
- [47] Shengfu Yang and Andrew M. Ellis. Helium droplets: a chemistry perspective. *Chem. Soc. Rev.*, 42(2):472–484, 2013.
- [48] M. Mudrich and F. Stienkemeier. Photoionisation of pure and doped helium nanodroplets. *International Reviews in Physical Chemistry*, 33(3):301–339, July 2014.
- [49] Chia K. Wang, Oleg Kornilov, Oliver Gessner, Jeong Hyun Kim, Darcy S. Peterka, and Daniel M. Neumark. Photoelectron imaging of helium droplets doped with xe and kr atoms†. *The Journal of Physical Chemistry A*, 112(39):9356–9365, October 2008.
- [50] F. Dong. Vibrational transition moment angles in isolated biomolecules: A structural tool. *Science*, 298(5596):1227–1230, November 2002.
- [51] K. K. Lehmann and G. Scoles. The ultimate spectroscopic matrix? *Science*, 279(5359):2065–2066, 1998.
- [52] M. Kelbg, M. Zabel, B. Krebs, L. Kazak, K.-H. Meiwes-Broer, and J. Tiggesbäumker. Auger emission from the coulomb explosion of helium nanoplasmas. *The Journal of Chemical Physics*, 150(20):204302, 2019.
- [53] Elastic electron-atom scattering cross-sections database at <http://www.ioffe.ru/ES/Elastic/>.